Dynamic and Collective Electrochemical Responses of Tetrathiafulvalene Derivative Self-Assembled Monolayers

Yasuyuki Yokota,[†,‡] Akira Miyazaki,[†] Ken-ichi Fukui,[†] Toshiaki Enoki,*[,†] Kaoru Tamada,[‡,§] and Masahiko Hara[‡,§]

Department of Chemistry, Graduate School of Science and Engineering, Tokyo Institute of Technology, Meguro-ku, Tokyo 152-8551, Japan, Local Spatio-Temporal Functions Laboratory, Frontier Research System, RIKEN (The Institute of Physical and Chemical Research), Wako, Saitama 351-0198, Japan, and Department of Electronic Chemistry, Interdisciplinary Graduate School of Science and Engineering, Tokyo Institute of Technology, Midori-ku, Yokohama 226-8502, Japan

Received: April 13, 2006; In Final Form: August 2, 2006

Electroactive tetrathiafulvalene (TTF)-containing alkanethiol self-assembled monolayers (SAMs) were designed and synthesized to elucidate the relationship between electrochemical responses and film structures. Two TTF derivative molecules having one alkanethiol chain (**1**) and two alkanethiol chains (**2**) were utilized to modulate the molecular packing arrangements in the SAMs, and the formation and structure of the SAMs were characterized by surface plasmon resonance spectroscopy (SPR). SPR measurements in various contacting media demonstrated loose packing of SAM **1** and close packing of SAM **2** due to the different space fillings of the molecules. Two successive one-electron redox waves were observed for both SAMs by cyclic voltammetry. The peak widths of the redox waves were strongly dependent on the oxidation states of the TTF moieties, the packing arrangement of the SAMs, and the contacting medium. We found that TTF-based SAMs exhibited collective electrochemical responses induced by dynamic structural changes, depending on the degree of freedom for the component molecules in the SAMs. These results imply that the molecular design, taking into account the electrochemical responses, extends the available range of molecular-based functionalities in TTF-based SAMs.

1. Introduction

Self-assembled monolayers (SAMs) of thiols on gold substrates have been studied extensively as a useful technique for surface fabrication.[1−3] Since the pioneering work of Chidsey,[4,5] a tremendous number of studies have been reported in the literature concerning electroactive SAMs of ferrocene-terminated alkanethiol.[6] They include kinetic and thermodynamic studies of electron transfer,[7] the properties of the electrical double layer,[8] and the influence of the redox microenvironment on electron transfer.[9] Among them, one of the most noticeable features is the ion-pairing ability of the oxidized species with counteranions.[10−12] Uosaki and co-workers, using a wide variety of surface science techniques, have revealed that such a process is frequently accompanied by the structural change of the SAMs (redox-induced orientational change).[13−15]

Recently, by changing the oxidation state of ferrocene-terminated SAMs triggered by an electrochemical potential, reversible controls of interfacial properties such as wettability[16] and the optical transparency of liquid crystals[17] have received considerable attention. From the perspective of molecular electronics controlled by an electrochemical potential, we have intensively studied tetrathiafulvalene (TTF)-terminated SAMs.[18,19] TTF can be easily oxidized in two successive one-electron steps into a stable monocation ($TTF^{\bullet+}$) and a dication (TTF^{2+}). Single-crystal forms of the radical ion salt and charge-transfer complex are well-known as typical organic conductors, and their high conductivity has been attributed to their electron donor ability and strong intermolecular interactions.[20,21] We have recently reported that by using in situ scanning tunneling microscopy (STM), an apparent height change of TTF derivative **1** embedded in *n*-decanethiol SAMs can be intentionally controlled by applying an electrochemical potential.[22] To construct a more complex system for further technical applications such as laterally conducting SAMs,[23,24] fundamental aspects of the electrochemical processes of TTF-terminated SAMs should be elucidated.

Many authors have reported the electrochemical properties of TTF derivative SAMs. Such studies include the redox activity of TTF derivatives on gold,[18,25,26] electrochemical polymerization,[27] double-layer capacitance,[28] metal ion recognition,[29−32] and host−guest complexation.[33,34] However, a microscopic understanding of the electrochemical processes of TTF-terminated SAMs has not yet been developed. For example, the peak width differences between the first and second redox reactions have been a controversial issue since Murray and co-workers reported the electrochemical properties of a TTF derivative immobilized on a metal oxide electrode in 1979.[35]

The objective of the present work was to provide a microscopic picture of the electrochemical processes of TTF derivative SAMs. We synthesized EDT-TTF(SCH_3)($SC_{11}H_{22}SH$) and EDT-TTF($SC_{11}H_{22}SH$)$_2$ (molecules **1** and **2**, respectively, shown in Chart 1) for elucidation of the relationship between the packing arrangements and electrochemical processes. The

* To whom correspondence should be addressed. E-mail: tenoki@chem.titech.ac.jp. Phone and fax: +81-3-5734-2242.

[†] Graduate School of Science and Engineering, Tokyo Institute of Technology.

[‡] RIKEN.

[§] Interdisciplinary Graduate School of Science and Engineering, Tokyo Institute of Technology.

10.1021/jp062285t CCC: $33.50
Published on Web 09/16/2006

CHART 1: TTF Derivatives EDT-TTF(SCH_3)($SC_{11}H_{22}SH$) and EDT-TTF($SC_{11}H_{22}SH$)$_2$ with One or Two Alkanethiol Chains

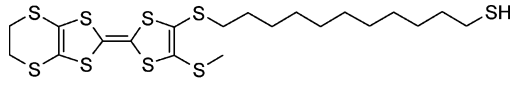

1

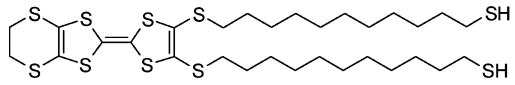

2

molecules have long alkyl spacer group(s) to electronically separate the TTF moiety from the metal substrate[36] and different alkyl chain numbers to modulate the packing arrangements of SAMs **1** and **2**. The formation and structure of the SAMs were characterized by surface plasmon resonance spectroscopy (SPR). Cyclic voltammetry (CV) was utilized to monitor the electrochemical processes.

2. Experimental Section

2.1. Materials. Milli-Q water (Nihon Millipore), redistilled perchloric acid (Aldrich), and electrochemical grade tetra-*n*-butylammonium perchlorate (TBAP) (Fluka) were used for the electrolyte solutions. All other commercial chemicals were of reagent grade or better. Dichloromethane for the electrochemical measurements was stored over activated molecular sieves (Wako Pure Chemicals) for at least 24 h.[37] All other chemicals were used without further purification. The TTF derivatives, compounds **1** and **2**, were synthesized according to the modification of reported procedures.[38] The synthetic route of molecule **1** is shown in Scheme 1, and that of molecule **2** is the same except that $-SCH_3$ is substituted with the corresponding $-SR$ groups. Starting materials 2-(2-cyanoethylthio)-6,7-(ethylenedithio)-3-(methylthio)tetrathiafulvalene (EDT-TTF(SCH_3)(SC_2H_4CN), **1a**) and 2,3-bis(2-cyanoethylthio)-6,7-(ethylenedithio)tetrathiafulvalene (EDT-TTF(SC_2H_4CN)$_2$, **2a**) were prepared according to the literature.[39]

*EDT-TTF(SCH_3)($SC_{11}H_{22}OH$) (**1b**)*. Compound **1a** (0.334 g, 0.785 mmol) and 28% sodium methoxide solution in methanol (0.32 mL) were stirred in ethanol (40 mL) for 4 h under Ar. Then 11-bromo-1-undecanol (1.58 g, 6.28 mmol) was added, and the solution was stirred for 12 h. The reaction mixture was poured into water (50 mL) and extracted with dichloromethane (50 mL × 2). A combined organic layer was washed with water (100 mL), dried over magnesium sulfate, and evaporated to dryness under reduced pressure. Silica gel column chromatography using toluene as an eluent yielded **1b** as an orange oil (0.162 g, 38.0%). ^{1}H NMR (270 MHz, $CDCl_3$): δ (ppm) 1.20−1.70 (m, 18H), 2.39 (s, 3H), 2.78 (t, 2H, J = 6.6 Hz), 3.27 (s, 4H), 3.62 (q, 2H, J = 5.5 Hz).

*EDT-TTF(SCH_3)($SC_{11}H_{22}SAc$) (**1c**)*. To a stirred solution of triphenylphosphine (0.273 g, 1.04 mmol) in THF (40 mL) at 0 °C under Ar was added diisopropyl azodicarboxylate (DIAD) (0.21 mL, 1.04 mmol). The mixture was stirred at 0 °C for 1 h. Compound **1b** (0.19 g, 0.35 mmol) in THF (20 mL) was added dropwise over 10 min, and the mixture was stirred for 1 h at room temperature. Thioacetic acid (0.074 mL, 1.04 mmol) was then added, and the solution was stirred for 12 h. The solution was concentrated and then purified by silica gel column chromatography using 50:50 dichloromethane/hexane as an eluent to give 0.082 g (39.4%) of **1c** as an orange oil. ^{1}H NMR (270 MHz, $CDCl_3$): δ (ppm) 1.20−1.70 (m, 18H), 2.33 (s, 3H), 2.41 (s, 3H), 2.80 (t, 2H, J = 7.3 Hz), 2.86 (t, 2H, J = 7.3 Hz), 3.30 (s, 4H).

*EDT-TTF(SCH_3)($SC_{11}H_{22}SH$) (**1**)*. To dry ether (50 mL) were added compound **1c** (0.20 g, 0.33 mmol) and lithium aluminum hydride (50.6 mg, 1.33 mmol). The solution was stirred under Ar for 30 min, and the excess lithium aluminum hydride was eliminated by the careful addition of a 1 M hydrochloric acid solution. The organic phase was dried over magnesium sulfate. The solution was concentrated and then purified by silica gel column chromatography using carbon disulfide as an eluent to give 0.159 g (83.8%) of **1** as an orange oil. ^{1}H NMR (270 MHz, $CDCl_3$): δ (ppm) 1.20−1.70 (m, 18H), 2.41 (s, 3H), 2.52 (q, 2H, J = 7.6 Hz), 2.80 (t, 2H, J = 7.3 Hz), 3.30 (s, 4H). Anal. Calcd for $C_{20}H_{30}S_9$: C, 42.97; H, 5.41; S, 51.62%. Found: C, 43.18; H, 5.32; S, 51.88%.

*EDT-TTF($SC_{11}H_{22}OH$)$_2$ (**2b**)*. Compound **2a** (1.6 g, 3.4 mmol) and 28% sodium methoxide solution in methanol (2.8 mL) were stirred in ethanol (40 mL) for 4 h under Ar. Then 11-bromo-1-undecanol (13.7 g, 54.4 mmol) was added, and the solution was stirred for 12 h. The reaction mixture was poured into water (50 mL) and extracted with dichloromethane (50 mL × 2). A combined organic layer was washed with water (100 mL), dried over magnesium sulfate, and evaporated to dryness under reduced pressure. The residue was washed with methanol to yield 1.64 g (68.8%) of **2b** as an orange solid. ^{1}H NMR (270 MHz, $CDCl_3$): δ (ppm) 1.20−1.70 (m, 36H), 2.80 (t, 4H, J = 7.2 Hz), 3.30 (s, 4H), 3.64 (q, 4H, J = 7.2 Hz). Anal. Calcd for $C_{30}H_{50}O_2S_8$: C, 51.53; H, 7.21; S, 36.68%. Found: C, 51.77; H, 7.48; S, 36.81%.

*EDT-TTF($SC_{11}H_{22}SAc$)$_2$ (**2c**)*. To a stirred solution of triphenylphosphine (2.0 g, 7.6 mmol) in THF (50 mL) at 0 °C under Ar was added DIAD (1.5 mL, 7.6 mmol). The mixture was stirred at 0 °C for 30 min. Compound **2b** (1.33 g, 1.9 mmol) in THF (50 mL) was added dropwise over 10 min. Thioacetic acid (0.6 mL, 7.6 mmol) was then added, and the solution was stirred for 1 h. The solution was concentrated and then purified by silica gel column chromatography using 50:50 dichloromethane/hexane as an eluent to give 0.516 g (33.3%) of **2c** as an orange solid. ^{1}H NMR (270 MHz, $CDCl_3$): δ (ppm) 1.20−1.70 (m, 36H), 2.32 (s, 6H), 2.80 (t, 4H, J = 8.0 Hz), 2.86 (t, 4H, J = 7.4 Hz), 3.30 (s, 4H).

*EDT-TTF($SC_{11}H_{22}SH$)$_2$ (**2**)*. To dry ether (50 mL) were added compound **2c** (0.14 g, 0.172 mmol) and lithium aluminum hydride (52.3 mg, 1.38 mmol). The solution was stirred under Ar for 30 min, and the excess lithium aluminum hydride was eliminated by the careful addition of a 1 M hydrochloric acid solution. The organic phase was dried over magnesium sulfate. The solution was concentrated and purified by silica gel column chromatography using carbon disulfide as an eluent to give 0.104 g (82.8%) of **2** as an orange solid. ^{1}H NMR (270 MHz, $CDCl_3$): δ (ppm) 1.20−1.70 (m, 36H), 2.52 (q, 4H, J = 7.4 Hz), 2.80 (t, 4H, J = 8.0 Hz), 3.30 (s, 4H). Anal. Calcd for $C_{30}H_{50}S_{10}$: C, 49.27; H, 6.89; S, 43.84%. Found: C, 49.26; H, 6.86; S, 43.58%.

2.2. Gold Substrates and Monolayer Preparation. Gold substrates were prepared by thermal deposition of gold metal on glass slides in a vacuum chamber at ~1 × 10^{-5} Pa (BIEMTRON Co. Ltd., Japan). The substrates for SPR measurements were ~50 nm thick gold on high-refractive index glass slides (LaSFN9, 25 × 35 mm^2). The substrates for the electrochemical measurements were 300 nm thick gold on glass slides precovered with 3 nm thick chromium adhesion layers.

For SAM formation, thiol solutions (0.1 mM acetone solution) were prepared. The SAMs for SPR measurements were prepared

SCHEME 1: Synthetic Route of Molecule 1[a]

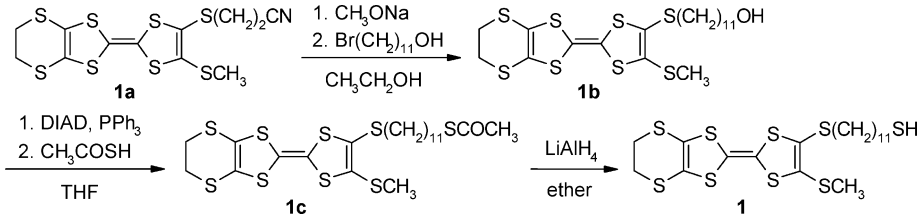

[a] The synthetic route of molecule **2** is the same except that $-SCH_3$ is substituted with the corresponding $-SR$ groups.

in situ by injection of the thiol solutions into the liquid cell. The SAMs for the electrochemical measurements were prepared by immersing gold substrates in the acetone solutions for at least 16 h, and the substrates were rinsed with absolute acetone and dried in a stream of N_2.

2.3. Surface Plasmon Resonance Spectroscopy.[40] The SPR measurement setup was based on the configuration introduced by Kretschmann and Raether.[41] The details of the experimental setup have been described elsewhere.[42] A 45° prism with high refractive index glass (LaSFN9, $n = 1.84$ at $\lambda = 632.8$ nm) was used, and all the liquid cells (internal volume ~3 mL) and the tubes were made of PTFE, which was resistant to organic solvents. A p-polarized laser beam (He−Ne, $\lambda = 632.8$ nm, maximum power 5 mW) was used as the light source, which was mechanically chopped before entry into the prism. The intensity of the beam reflected at the gold interface was detected by a photodiode detector in conjunction with a lock-in amplifier and recorded as a function of the incidence angle for "angular-scan" measurements or as a function of time at a fixed angle of incidence for "kinetics-scan" measurements.

The thickness and complex refractive index of the gold layer were determined by curve fitting of the SPR data (angular scan) in absolute acetone.[43] The SAM formation was initiated by injection of the 4 mL thiol solution (0.1 mM acetone solution) into the cell, and the adsorption process was monitored via the change of reflectivity by the kinetics-scan measurement (incidence angle 58°). The adsorption was continued for at least 16 h, after which the surface was rinsed with absolute acetone. The angular-scan measurements were carried out in various solvents (acetone, methanol, hexane, acetonitrile, and dichloromethane) and in air for independent determination of the thicknesses and refractive indices of the SAMs.[44,45] During this procedure, one solvent was successively replaced by another solvent, and the measurements with acetone were performed several times intermittently to confirm that there was no damage to or contamination on the SAM due to exposure to the new solvents. The refractive index of each solvent was obtained from the critical angle for total internal reflection in the SPR curve with SAMs for each measurement.

2.4. Electrochemical Measurements. For the electrolyte solutions, a 0.1 M TBAP/dichloromethane solution and a 0.5 M $HClO_4$ aqueous solution were prepared. Prior to the electrochemical measurements, the electrolyte solutions were deaerated for at least 20 min with N_2 gas. The electrode potential was controlled by a potentiostat (HAB-151, Hokuto Denko). A three-electrode, two-compartment cell was used for the electrochemical measurements.[11] Ag/AgCl (3.0 M NaCl) and Ag/Ag^+ (0.1 M TBAP/acetonitrile) were used as the reference electrodes for aqueous and organic solutions, respectively. Pt wire was used as the counter electrode. The geometric area of the working electrode was ~0.28 cm^2. The roughness factor of the gold surface was determined from the charge required for the formation and reduction of gold oxide in $HClO_4$ solution and was 1.9 ± 0.1.[46] This roughness was used in all calculations of surface coverage. Electrochemical measurements of TTF compounds dissolved in dichloromethane solution were performed using a glassy carbon electrode (~0.07 cm^2).

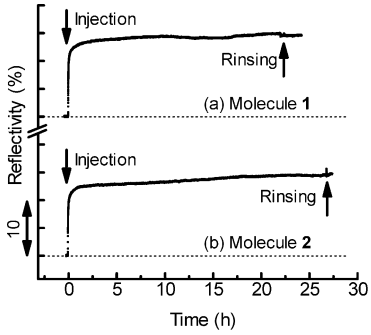

Figure 1. Adsorption kinetics of molecules **1** (a) and **2** (b) on gold from 0.1 mM acetone solution. Down- and up-arrows indicate the times at which the sample solution was injected and the sample was rinsed with pure acetone, respectively. Horizontal dotted lines represent the reflectivity before injection.

2.5. Molecular Modeling. Geometrically optimized chemical structures of molecules **1** and **2** were calculated using MOPAC 6.0 (AM1) and displayed using Facio software.[47] The initial geometry of molecule **2** for geometry optimization was estimated from an optimized structure of disulfide derivative EDT-TTF$(SC_{11}H_{22}S)_2$ to be converged.

3. Results and Discussion

3.1. Surface Plasmon Resonance Spectroscopy. The self-assembly processes of molecules **1** and **2** were examined by kinetics-scan measurements. After the reflectivity became unchanged with time in pure acetone, the acetone solution of molecule **1** or **2** was injected, and the reflectivity was monitored as shown in Figure 1. During the first 1 h, the reflectivity steeply increased upon injection, followed by a gradual increase, and reached a constant value within 12 h for **1** and 16 h for **2**. This two-step kinetics for the thiol adsorption is similar to that of ordinary *n*-alkanethiol SAMs.[48] Almost no change in reflectivity was observed upon rinsing with acetone, indicating that molecules **1** and **2** formed quite stable SAMs and that almost no desorption of molecules **1** and **2** took place by rinsing. The above observation is quite contrary to the case of EDT-TTF-$(SC_{11}H_{22}OH)_2$.[49] There is no significant reflectivity change upon its injection, although it has eight sulfur atoms expected to interact with the gold substrate. Hence, the presence of thiol functional groups is crucial to the formation of high-density SAMs.

We executed a reliable analysis for the determination of the SAM thickness by a contrast variation technique, that is, the determination of both the refractive index (n) and the thickness (d) of the SAM from the SPR data taken in various solvents (in media with different refractive indices). Figure 2 shows the simulation results of n and d estimated from the SPR peak shift by an angular scan in various media. If there is no solvent effect

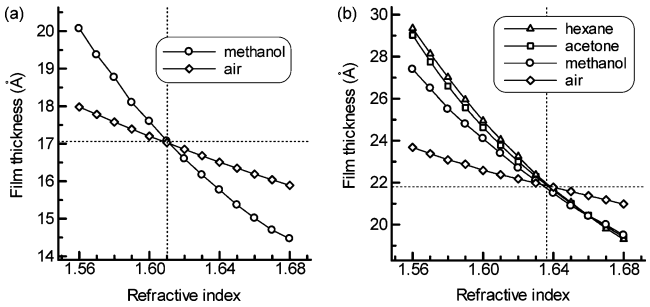

Figure 2. Film thicknesses versus refractive indices determined by a contrast variation SPR technique for SAM **1** (a) and SAM **2** (b) in various media. Dotted lines indicate the real film thickness and refractive index, which were determined in consideration of the curve-fitting error of angular-scan data.

TABLE 1: Estimation of the Refractive Index and Film Thickness of SAM Layers and Comparison to the Molecular Length

sulfur compd	refractive index	film thickness (Å)	molecular length[a] (Å)
1	1.61 ± 0.01	17.1 ± 0.5	27
2	1.63 ± 0.01	21.7 ± 0.5	27

[a] The molecular length is estimated from the molecular model shown in Figure 3a.

such as swelling in poor solvents, the curves should intersect at one point, which indicates the actual values of n and d of the SAM.[48] For SAM **2**, the intersection of the methanol, acetone, hexane, and air curves was obtained reproducibly, and the refractive index and the thickness were estimated to be $n = 1.63 \pm 0.01$ and $d = 21.7 \pm 0.5$ Å, respectively. On the other hand, none of the media except for methanol and air allowed us to obtain reproducible angular-scan data for SAM **1**. The refractive index and the thickness of SAM **1** were estimated from the intersection of the methanol and air curves to be $n = 1.61 \pm 0.01$ and $d = 17.1 \pm 0.5$ Å, respectively.

3.2. Structural Model of Neutral TTF SAMs. The film thickness and refractive index of SAMs **1** and **2** are summarized in Table 1 together with the molecular length of each component, where the molecular length is obtained from AM1 semiempirical calculations (Figure 3a). Whereas molecules **1** and **2** have almost the same molecular length, the film thickness differs considerably between SAMs **1** and **2**. The ratios of the film thickness to the molecular length are approximately 63% and 80% for SAMs **1** and **2**, respectively. We estimate the size of molecules **1** and **2** to interpret the origin of the different film thicknesses. It is obvious from the left side of Figure 3b that the TTF moiety of molecule **1** determines the maximum cross sectional area normal to the long axis. In contrast, two alkyl chains determine the maximum cross sectional area instead of the TTF moiety for the case of molecule **2**, as clearly shown on the right side of Figure 3b. We therefore suggest that the thinner film thickness of SAM **1** compared to SAM **2** obtained from $n-d$ plots in poor solvents can be attributed to the molecular tilt of molecule **1** to reduce the free space in the alkyl chain part. The refractive index data suggest comparable film densities of SAMs **1** and **2**, which support our assumption described above.

The relevance of the obtained refractive indices is discussed here. We expected the refractive indices of SAMs **1** and **2** to be between 1.5 and 1.6, because (i) 1.45 or 1.50 has been used as the refractive index of *n*-alkanethiol SAMs[1,50,51] and (ii) 1.60 or 1.62 has been reported to be the refractive index of evaporated films of TTF derivatives.[18,52] Refractive indices larger than 1.60 can be rationalized by the optical anisotropy of molecules **1** and **2**. The refractive index along the long axis of the TTF backbone, $n_{\|}$, has a larger value than that along the short axes, $n_{\perp}$, because the polarization is related to how far the charge is modulated against the external field.[53] In fact, Seed et al. have reported that some TTF-based liquid crystals show very large optical anisotropy, on the basis of the use of an Abbé refractometer.[54] In the case of optical measurements for an evaporated TTF film, random molecular orientations orientationally average the refractive index between $n_{\|}$ and $n_{\perp}$, resulting in an isotropic refractive index. However, the isotropic condition is disrupted in the case of SPR measurements of SAMs composed of optically anisotropic molecules. The smaller the tilt angles, the more $n_{\|}$ contributes to n_z (the z axis is perpendicular to the surface), giving a larger refractive index. Because p-polarized incident light is only influenced by n_x and n_z (the incident plane is the $x-z$ plane), the contribution from $n_{\|}$ is enhanced in the SPR measurements. Hence, the large refractive indices prove that the average tilt angle of the TTF moiety long axis is small in TTF-based SAMs having large optical anisotropy. This finding is consistent with that predicted by the structural model discussed above (slightly tilted but basically aligned normal to the surface).

We performed one more SPR measurement in good solvents to confirm the swelling effect.[55] We characterized the angular-scan data of SAM **2** in acetonitrile and dichloromethane. Figure 4 shows the $n-d$ plots in these solvents in addition to those of acetone and air for comparison. The $n-d$ plots of acetonitrile and dichloromethane deviate considerably from the intersection of acetone and air, thus suggesting that the optical properties of SAM **2** in acetonitrile and dichloromethane differ from those of the other solvents shown in Figure 2b. The shift of the $n-d$ curves to the upper right direction indicates that the apparent refractive index of SAM **2** increases by intercalation of the solvent molecules into the free space of SAM **2** and/or that the orientational change of the TTF moiety in SAM **2** is induced by solvent intercalation. It should be noted that acetonitrile has a high affinity for the TTF moiety and that dichloromethane has one of the highest solubilities of molecule **2**. When the solvent was replaced with acetone, the situation depicted in Figure 2b was reproduced. The lack of reproducibility for SAM **1** (data not shown) can also be interpreted on the basis of the above consideration. Because the solubility of molecule **1** in the solvents investigated is higher than that of molecule **2**, it is expected that the solvent effect for SAM **1** would be larger than that for SAM **2**. Furthermore, the less ordered structure of SAM **1**, as mentioned above, may result in a complicated solvent intercalation and its hysteresis. The reproducible intersection between air and methanol might result from hydrogen bonding preventing the methanol molecules from intercalating into the hydrophobic SAM **1**.

On the basis of these SPR data, we can draw a structural model of neutral SAMs **1** and **2** with their solvent effects. In the case of SAM **2** in poor solvents (air, methanol, acetone, and hexane), the film structure is not largely influenced by contacting solvents, giving a well-determined intersection in the $n-d$ plots. However, the influence of solvent is not negligible in the case of good solvents (acetonitrile and dichloromethane). In contrast, in the case of SAM **1**, only methanol and air gave a reproducible intersection, indicating a pronounced solvent effect derived from the less dense film structure and/or the higher solubility of the constituent molecule. The experimental findings can be summarized by saying that the structural degree

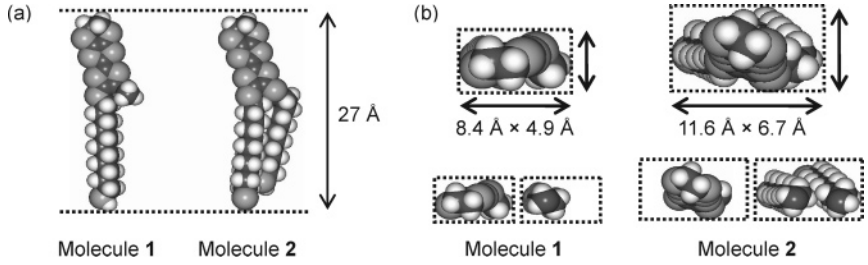

Figure 3. (a) Molecular configurations of molecules **1** and **2** obtained from AM1 semiempirical calculations. (b) Size estimation of molecules **1** and **2**. Molecular conformations are viewed along with the molecular axis to minimize the projection area. The projection area of molecule **1** is determined by a bulky TTF moiety, whereas that of molecule **2** is mainly determined by two alkyl chains. The TTF moieties of molecules **1** and **2** are defined as EDT-TTF(SCH_3)(SCH_2-) and EDT-TTF(SCH_2-)$_2$, respectively.

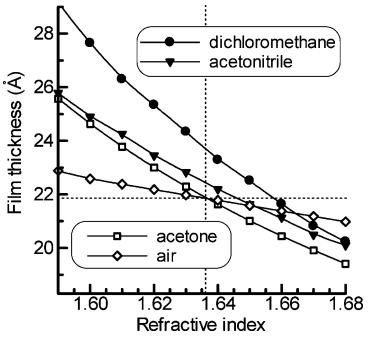

Figure 4. Film thicknesses versus the refractive indices for SAM **2** in contact with good solvents, dichloromethane and acetonitrile, in addition to acetone and air. The intersection of the plots of acetone and air represents the real film thickness (horizontal dotted line) and refractive index (vertical dotted line) determined in Figure 2b.

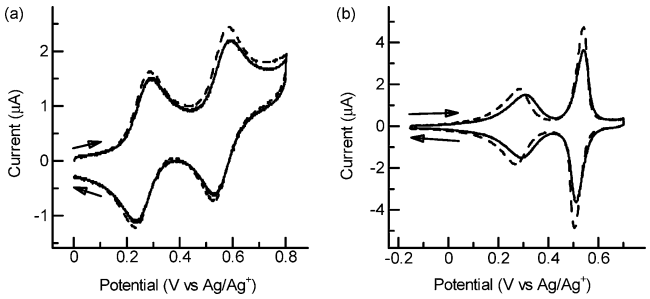

Figure 5. Cyclic voltammograms of 0.1 mM molecule **1** (dashed line) and molecule **2** (solid line) in 0.1 M TBAP/dichloromethane solution at a glassy carbon electrode (a) and of SAM **1** (dashed line) and SAM **2** (solid line) in 0.1 M TBAP/dichloromethane (b). The potential scan rate is 0.02 V/s.

of freedom in neutral SAMs changes with the number of alkyl chains and the contacting medium.

3.3. Electrochemistry of Molecules 1 and 2 Dissolved in Dichloromethane. Figure 5a shows cyclic voltammograms of molecules **1** and **2** in 0.1 M TBAP/dichloromethane solution at a glassy carbon electrode. The TTF backbones of molecules **1** and **2** undergo two successive reversible one-electron redox reactions, giving two pairs of well-defined redox peaks with peak-to-peak separations (ΔE_p) of ca. 60 mV. The first and second peaks appear at $E_1^{1/2} = 0.26$ V and $E_2^{1/2} = 0.56$ V vs Ag/Ag^+, respectively, for both molecules, as summarized in Table 2. The same electrochemical behavior of the two molecules indicates the same electronic structures and diffusion coefficients.[56] The former was confirmed by UV−vis spectra of the two molecules (data not shown), which is consistent with the similar electron-donating ability of the $-SCH_3$ and $-SC_{11}H_{22}SH$ groups. The latter might imply that two molecules

TABLE 2: Comparison of Redox Potentials of SAMs 1 and 2 in Dichloromethane Solution[a]

	redox potential (V vs Ag/Ag^+)	
SAM	first peak	second peak
1	0.27 (0.26)	0.51 (0.56)
2	0.30 (0.26)	0.52 (0.56)

[a] Values in parentheses correspond to the redox potentials of molecules **1** and **2** dissolved in dichloromethane.

dissolved in dichloromethane have approximately the same dimensions in terms of diffusion processes.[53] On the basis of these results, we could conclude that molecules **1** and **2** have almost the same electrochemical properties in dichloromethane solution.

3.4. Electrochemical Properties of SAMs. Figure 5b shows cyclic voltammograms of SAMs **1** and **2** in 0.1 M TBAP/dichloromethane. The TTF backbones of SAMs **1** and **2** undergo two one-electron redox processes, giving two pairs of well-defined redox peaks. The peak current is found to be proportional to the scan rate (data not shown), indicating a "surface wave" response.[56] Table 2 summarizes the redox potentials of SAMs **1** and **2**. The first and second peaks of SAM **1** appear at $E_1^{1/2} = 0.27$ V and $E_2^{1/2} = 0.51$ V vs Ag/Ag^+, respectively. Those of SAM **2** appear at $E_1^{1/2} = 0.30$ V and $E_2^{1/2} = 0.52$ V vs Ag/Ag^+, respectively. The shape of both cyclic voltammograms was not changed by repeating the potential cycles for our usual experimental duration (∼1 h), provided that the electrolyte solutions used were not contaminated by water, halogen impurities, and so on.[37]

Here we discuss the relationship between film structure and electrochemical processes on the basis of the comparison of the coverages, redox potential, and full width at half-maximum (fwhm) between SAMs **1** and **2**.

First, the experimentally obtained coverages are compared to the theoretically calculated coverages to elucidate how densely the constituent molecules are packed. The surface coverages of SAMs **1** and **2**, obtained by integration of the current and corrected by the roughness factor, are $(2.4 \pm 0.1) \times 10^{-10}$ and $(2.1 \pm 0.1) \times 10^{-10}$ mol/cm^2, respectively. We tentatively assume the shapes of molecules **1** and **2** to be rectangular blocks, 8.4×4.9 and 11.6×6.7 Å^2 in size (Figure 3b), respectively, with orthogonal close-packing. From this assumption, the calculated maximum coverages of SAMs **1** and **2** are estimated to be 3.9×10^{-10} and 2.1×10^{-10} mol/cm^2, respectively. The latter is in good agreement with the experimentally obtained coverage, which includes the uncertainty in the true surface area and the presence of disorder in the SAM. In contrast, the experimentally obtained coverage of SAM **1** is smaller than the calculated maximum coverage, however, the free space is reduced by the tilt of molecule **1** as indicated in the smaller

TABLE 3: Comparison of FWHM Values Estimated from CV Measurements in Different Media

	fwhm (mV) in dichloromethane		fwhm (mV) in aqueous solution[a]	
SAM	first peak	second peak	first peak	second peak
1	130 ± 8	47 ± 2	>200[b]	~60
2	140 ± 7	56 ± 2	~150	~70

[a] Estimation of the fwhm values is perturbed by superposition of the first and second peaks. [b] The peak is not well-defined.

film thickness determined by SPR measurements. Hence, from the perspective of the packing arrangement of the molecules, SAM **2** is considered to form densely packed SAMs, although the coverage itself is larger for SAM **1**.

Second, our discussion focuses on the redox potentials of SAMs **1** and **2** in dichloromethane to deduce the environment of the TTF moiety. The first redox potential ($TTF \leftrightarrow TTF^{\bullet+}$) of SAM **2** is different from that of SAM **1**. This difference is not caused by the difference in individual molecular properties, since the redox potentials of molecules **1** and **2** in solution are the same, as discussed in the previous section. It is well-known that the redox potential of a SAM is dependent on the surrounding environment of the redox-active moiety in the SAM. Creager and Rowe have systematically investigated ferrocene-terminated SAMs surrounded by ω-functional alkanethiol SAMs having various chain lengths, suggesting that a hydrophobic environment (i.e., embedded in a long alkanethiol) impedes ferrocene oxidation, which leads to a higher redox potential.[9] Thus, the close proximity of the first redox potential of SAM **1** and that of molecule **1** in dichloromethane solution (see Table 2) indicates that the TTF moieties in SAM **1** are in the same environment as in solution. This result is consistent with the higher solvent permeability into SAM **1**, as determined by the SPR measurements. In contrast, the first redox potential of SAM **2** is shifted to the high redox potential range from that of molecule **2**, as shown in Table 2. This shift implies that the surrounding molecules **2** prevent the solvent molecules from adequately stabilizing the oxidation state of the TTF moiety.[6] The second redox potentials ($TTF^{\bullet+} \leftrightarrow TTF^{2+}$) of SAMs **1** and **2** are lower than those of molecules **1** and **2** in solution, which indicates that the TTF moieties of the SAM are more easily oxidized than those in solution. This surprising and complicated situation will be discussed later.

The third issue is fwhm values of SAMs **1** and **2** in dichloromethane. The fwhm in an ideal case, where an ideal Nernstian reaction under the Langmuir isotherm conditions occurs at 25 °C, is ca. 90 mV,[56] and the deviation from the fwhm in the ideal CV diagnostics reveals details about the redox center.[6] In both SAMs **1** and **2** in dichloromethane, fwhm values of the first redox peaks were larger than 90 mV, whereas those of the second redox peaks were smaller than 90 mV, as shown in Table 3. The large fwhm values of the first redox peaks suggest the presence of a distribution of redox potentials (a distribution of local environments about the redox centers), although the contribution of other factors might be included (i.e., repulsive interaction[6] and double-layer effects[8]). We will discuss the solvent effect later in relation to the distribution of local environments. The small fwhm values of the second peaks suggest that the TTF moieties attractively interact with each other in the second redox process.

Using the model of interaction originally introduced by Brown and Anson,[57] we analyze the potential and fwhm of the second redox peak to elucidate the electrochemical process of SAMs **1** and **2**. According to Brown and Anson, the interaction parameter describes the perturbing influence experienced by a given molecule of attached oxidant or reductant due to the presence of the other attached oxidant and reductant molecules. They described the ratio of oxidant and reductant activities as

$$\frac{a_O}{a_R} = \frac{\Gamma_O \exp\{-(\gamma_{OO}\Gamma_O + \gamma_{OR}\Gamma_R)\}}{\Gamma_R \exp\{-(\gamma_{RR}\Gamma_R + \gamma_{RO}\Gamma_O)\}} \quad (1)$$

where a and Γ are the surface activities and concentrations, respectively; the subscripts indicate the oxidized (O) and reduced (R) forms of the adsorbate. γ_{ij} is the interaction parameter that describes the perturbing influence experienced by species i due to the presence of species j. By using the Nernst equation and eq 1, the peak current and potential are expressed as

$$I_{peak} = \frac{n^2F^2Av\Gamma_T}{RT\{4 - \Gamma_T(\gamma_R + \gamma_O)\}} \quad (2)$$

$$E_{peak} = E^{1/2} + \frac{RT}{2nF}\Gamma_T(\gamma_R - \gamma_O) \quad (3)$$

where γ_O and γ_R are defined as $\gamma_O = \gamma_{OO} - \gamma_{RO}$ and $\gamma_R = \gamma_{RR} - \gamma_{OR}$, respectively, n is the number of electrons transferred in the reaction, F is the Faraday constant, A is the electrode surface area, v is the scan rate, Γ_T is the total surface coverage, and the other parameters have their usual meanings. By using the redox potentials of molecules **1** and **2** dissolved in solution as $E^{1/2}$ and the experimentally obtained coverages as Γ_T, γ_O and γ_R of SAM **1** are estimated to be 1.2×10^{10} and -4.7×10^9 cm^2/mol, respectively, and those of SAM **2** to be 1.0×10^{10} and -4.4×10^9 cm^2/mol, respectively. Because the electrode potential is expressed as

$$E = E^{1/2} + \frac{RT}{nF}(\gamma_R\Gamma_R - \gamma_O\Gamma_O) + \frac{RT}{nF}\ln\frac{\Gamma_O}{\Gamma_R} \quad (4)$$

the second term, which depends on the interaction parameter, shifts the apparent redox potential E. As $\gamma_R < 0$, the apparent redox potential is negatively shifted *before* the second redox reaction ($\Gamma_R = \Gamma_T$). This shift indicates that monocation TTF moieties in the SAMs after the first oxidation reaction are in a more reactive environment than in solution. Furthermore, as $\gamma_O > 0$, $\gamma_R < 0$, and $|\gamma_O| > |\gamma_R|$ in our cases, when the redox reaction proceeds, the more negatively shifted apparent redox potential accelerates the reaction, resulting in narrower fwhm values than in the ideal case.

What is the microscopic origin of the reaction acceleration? It is well-known that when redox reactions of the terminal groups create or annihilate charges at the monolayer/solution interface, the formation or dissociation of ion pairs occurs.[10−12] Such a process is frequently accompanied by a structural change of the SAM due to the energetically unfavorable environment of the charged species.[13−15] Because the ion pairing itself does not change the fwhm, it should facilitate the neighboring redox reaction to narrow the fwhm. Sato and Uosaki have reported that a counterion-mediated attractive interaction between ferricinium moieties results in a narrow fwhm, and a disorganized monolayer does not show this narrowing.[58] In our case, the first redox reaction of the TTF moieties occurred in various environments due to the disorganized monolayer of neutral TTF molecules, as judged from the large fwhm. Hence, we rationalize the experimental observation by the following successive oxidation processes (Figure 6). (1) Neutral TTF moieties in various environments oxidize. Charge creation in TTF moieties leads

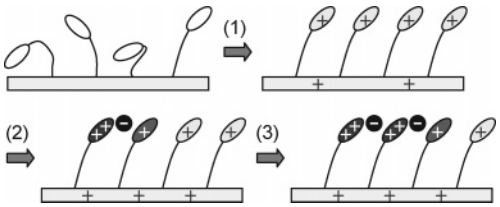

Figure 6. Schematic illustrations of electrochemical processes of SAM **1** in dichloromethane. These hold for SAM **2** and in aqueous solution except for the different restrictions of structural change due to the different structural degrees of freedom in the SAMs. (1) Neutral TTF moieties in various environments oxidize. Charge creation in TTF moieties leads to the formation of ion pairs (the counteranions appearing after the first oxidation of TTF moieties are omitted for clarity) and changes the orientation of the $TTF^{\bullet+}$ moieties to a more homogeneous environment. (2) The $TTF^{\bullet+}$ moiety oxidizes to TTF^{2+} and attracts anions. (3) The anion facilitates the reaction of the neighboring $TTF^{\bullet+}$ moieties by raising the local electrostatic potential of the electron.

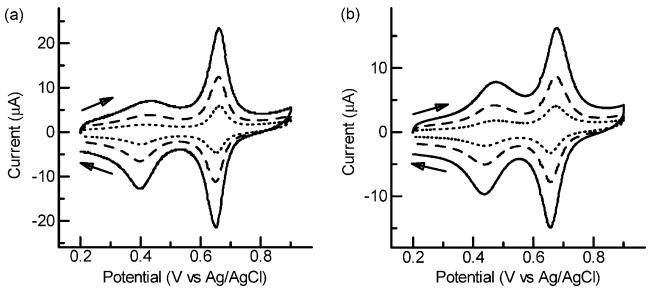

Figure 7. Cyclic voltammograms of SAM **1** (a) and SAM **2** (b) in 0.5 M $HClO_4$. The potential scan rates are 0.1 V/s (solid line), 0.05 V/s (dashed line), and 0.02 V/s (dotted line).

to the creation of ion pairs and changes the orientation of $TTF^{\bullet+}$ moieties to a more homogeneous environment. (2) The $TTF^{\bullet+}$ moiety oxidizes to TTF^{2+} and attracts anions. (3) The anion facilitates the reaction of the neighboring $TTF^{\bullet+}$ moieties by raising the local electrostatic potential of the electron.

As clearly shown in Figure 5b, the fwhm of the second redox peak of SAM **1** is narrower than that of SAM **2** (Table 3). This narrowing demonstrates that the reaction acceleration by ion pairs, that is, the counterion-mediated attractive interaction, is more efficient in SAM **1** than in SAM **2**. As discussed in the SPR results, the swelling of SAM **1** due to the permeation of dichloromethane is more significant than that of SAM **2**. This difference suggests that the structural degree of freedom in the monolayer is higher in SAM **1**. It therefore appears that the TTF moieties in SAM **1** can be loosely organized in a plane, in which the counterion-mediated attractive interaction operates well. On the other hand, the interaction, although it exists, is not allowed to operate in the close-packed SAM **2** due to its low structural degree of freedom. An interesting feature of these systems is that dynamic structural changes after the first oxidation, which are an arbitrary behavior of individual molecules, result in collective electron-transfer responses in the second redox reaction. Such a feature is more prominent for loosely packed (i.e., more dynamic) SAM **1**.

We also performed CV measurements using aqueous solution as an electrolyte to confirm the above discussion. Figure 7 shows cyclic voltammograms of SAMs **1** and **2** in 0.5 M $HClO_4$ aqueous solution. The TTF backbones of SAMs **1** and **2** in water also gave two redox peaks, but they were less well-defined than those in dichloromethane. The peak current was found to be proportional to the scan rate, indicating a surface wave response. The first and second redox potentials of SAM **1**, calculated from the average of the peak potentials of oxidation and reduction, appear at $E_1^{1/2} = 0.41$ V and $E_2^{1/2} = 0.66$ V vs Ag/AgCl, respectively. Those of SAM **2** appear at $E_1^{1/2} = 0.46$ V and $E_2^{1/2} = 0.67$ V vs Ag/AgCl, respectively. The surface coverages of SAMs **1** and **2** are almost the same as in dichloromethane. It should be noted that the first oxidation peak of SAM **1** is remarkably deformed and broadened, indicating a wide distribution of redox potentials related to various local environments of neutral TTF moieties. This phenomenon appears to be the result of a disorganized and compacted monolayer due to the contact with a poor solvent. After oxidation, the TTF moieties of SAM **1** in water gave a well-defined redox peak, indicating a structural change to a structure having better regularity in SAM **1**.

The tendency for the second peak fwhm of SAM **1** in dichloromethane to be narrower than that of SAM **2** is preserved in aqueous solution, as summarized in Table 3. Furthermore, compared to the case in dichloromethane, the second peak fwhms of SAMs **1** and **2** in water are broadened, although narrower than the ideal case (90 mV). We consider that the structural degree of freedom in the SAMs is reduced in aqueous solution, which might be due to the hydrophobicity of the alkyl chains in the SAMs.

We have recently reported in situ STM studies of molecule **1** islands embedded in *n*-decanethiol SAMs, in which the apparent height changes were observed depending on the electrode potential and island size.[22] Briefly, large islands were invariably protruding against the surrounding area, whereas small islands changed their apparent height depending on the oxidation state of the TTF moieties. We attributed the former behavior to the structural rigidity in the large island due to a TTF stacking effect (low structural degree of freedom), while the latter behavior appeared to be due to a redox-induced orientational change caused by less effective TTF stacking in the small islands (high structural degree of freedom). The size-dependent behavior is qualitatively consistent with the present structural and electrochemical study of the SAMs having different structural degrees of freedom depending on the alkyl chain numbers and contacting media. In situ optical measurements are necessary to provide a quantitative understanding of the structure of the TTF-based SAMs under electrochemical processes.

4. Conclusions

The properties of SAMs **1** and **2** on gold substrates, particularly dynamic electrochemical processes, were characterized using SPR and CV techniques. In these studies, we found that differences in the numbers of alkanethiol chains (one or two chains) in a molecule and contacting medium have a pronounced influence on the molecular arrangement and electrochemical responses in SAMs. The SPR contrast variation technique revealed that the presence of two alkanethiol chains in molecule **2** resulted in a lower structural degree of freedom in SAM **2** compared with SAM **1**, and the structural degree of freedom in both SAMs was affected by the contacting medium depending on its affinity for molecules **1** and **2**. Two successive one-electron redox waves were observed for both SAMs in CV. The peak widths of the redox waves, which reflect the microscopic electrochemical processes, were found to be strongly dependent on the oxidation state of the TTF moieties, the packing arrangement of the SAMs, and the contacting medium. A new important insight gained from this variety of comparisons is that TTF-based SAMs exhibit dynamic and collective electrochemical responses, depending on the structural degree of freedom in the

SAMs. Furthermore, loosely packed SAM **1** showed more collective behavior than close-packed SAM **2**. This knowledge will undoubtedly prove useful in designing and fabricating molecular devices controlled by an electrochemical potential.

Acknowledgment. We are grateful to Dr. T. Murase and Dr. N. Fukuda for their advice concerning the electrochemical measurements. We acknowledge Dr. M. Inakuma, Dr. K. Takai, Dr. T. Isoshima, and Dr. E. Ito for fruitful discussions. Y.Y. thanks Dr. R. Yuge and Dr. S. Yokokawa for their kind help with the SPR measurements. This work was financially supported by Grants-in-Aid (No. 15073211, No. 17034014, and 21st Century COE Program "Creation of Molecular Diversity and Development of Functionalities") from the Ministry of Education, Culture, Sports, Science and Technology, Japan. Y.Y. thanks RIKEN for the JRA fellowship.

References and Notes

(1) Ulman, A. *An Introduction to Ultrathin Organic Films from Langmuir−Blodgett to Self-Assembly*; Academic Press: New York, 1991.
(2) Ulman, A. *Chem. Rev.* **1996**, *96*, 1533.
(3) Love, J. C.; Estroff, L. A.; Kriebel, J. K.; Nuzzo, R. G.; Whitesides, G. M. *Chem. Rev.* **2005**, *105*, 1103.
(4) Chidsey, C. E. D.; Bertozzi, C. R.; Putvinski, T. M.; Mujsce, A. M. *J. Am. Chem. Soc.* **1990**, *112*, 4301.
(5) Chidsey, C. E. D. *Science* **1991**, *251*, 919.
(6) Finklea, H. O. In *Electroanalytical Chemistry*; Bard, A. J., Rubinstein, I., Eds.; Marcel Dekker: New York, 1996; Vol. 19, pp 109−335.
(7) Richardson, J. N.; Peck, S. R.; Curtin, L. S.; Tender, L. M.; Terrill, R. H.; Carter, M. T.; Murray, R. W.; Rowe, G. K.; Creager, S. E. *J. Phys. Chem.* **1995**, *99*, 766.
(8) Smith, C. P.; White, H. S. *Anal. Chem.* **1992**, *64*, 2398.
(9) Rowe, G. K.; Creager, S. E. *J. Phys. Chem.* **1994**, *98*, 5500.
(10) Uosaki, K.; Sato, Y.; Kita, H. *Langmuir* **1991**, *7*, 1510.
(11) Creager, S. E.; Rowe, G. K. *Anal. Chim. Acta* **1991**, *246*, 233.
(12) De Long, H. C.; Donohue, J. J.; Buttry, D. A. *Langmuir* **1991**, *7*, 2196.
(13) Ohtsuka, T.; Sato, Y.; Uosaki, K. *Langmuir* **1994**, *10*, 3658.
(14) Ye, S.; Sato, Y.; Uosaki, K. *Langmuir* **1997**, *13*, 3157.
(15) Ye, S.; Haba, T.; Sato, Y.; Shimazu, K.; Uosaki, K. *Phys. Chem. Chem. Phys.* **1999**, *1*, 3653.
(16) Yamada, R.; Tada, H. *Langmuir* **2005**, *21*, 4254.
(17) Luk, Y.-Y.; Abbott, N. L. *Science* **2003**, *301*, 623.
(18) Yuge, R.; Miyazaki, A.; Enoki, T.; Tamada, K.; Nakamura, F.; Hara, M. *J. Phys. Chem. B* **2002**, *106*, 6894.
(19) Yuge, R.; Miyazaki, A.; Enoki, T.; Tamada, K.; Nakamura, F.; Hara, M. *Jpn. J. Appl. Phys.* **2002**, *41*, 7462.
(20) Williams, J. M.; Ferraro, J. R.; Thorn, R. J.; Carlson, K. D.; Geiser, U.; Wang, H. H.; Kini, A. M.; Whangbo, M.-H. *Organic Superconductors (Including Fullerenes): Synthesis, Structure, Properties, and Theory*; Prentice Hall: Englewood Cliffs, NJ, 1992.
(21) Ishiguro, T.; Yamaji, K.; Saito, G. *Organic Superconductors*, 2nd ed.; Fulde, P., Ed.; Springer Series in Solid-State Sciences; Springer-Verlag: Berlin, 1998; Vol. 88.
(22) Yokota, Y.; Miyazaki, A.; Fukui, K.; Enoki, T.; Hara, M. *J. Phys. Chem. B* **2005**, *109*, 23779.
(23) Ishida, T.; Mizutani, W.; Akiba, U.; Umemura, K.; Inoue, A.; Choi, N.; Fujihira, M.; Tokumoto, H. *J. Phys. Chem. B* **1999,** *103*, 1686.
(24) Fan, F.-R. F.; Yang, J.; Cai, L.; Price, D. W., Jr.; Dirk, S. M.; Kosynkin, D. V.; Yao, Y.; Rawlett, A. M.; Tour, J. M.; Bard, A. J. *J. Am. Chem. Soc.* **2002,** *124*, 5550.
(25) Yip, C. M.; Ward, M. D. *Langmuir* **1994**, *10*, 549.
(26) Pacsial, E. J.; Alexander, D.; Alvarado, R. J.; Tomasulo, M.; Raymo, F. M. *J. Phys. Chem. B* **2004**, *108*, 19307.
(27) Fujihara, H.; Nakai, H.; Yoshihara, M.; Maeshima, T. *Chem. Commun.* **1999**, 737.
(28) Petoral, R. M., Jr.; Wermelin, K.; Dahlstedt, E.; Hellberg, J.; Uvdal, K. *J. Colloid Interface Sci.* **2005**, *287*, 388.
(29) Moore, A. J.; Goldenberg, L. M.; Bryce, M. R.; Petty, M. C.; Monkman, A. P.; Marenco, C.; Yarwood, J.; Joyce, M. J.; Port, S. N. *Adv. Mater.* **1998**, *10*, 395.
(30) Moore, A. J.; Goldenberg, L. M.; Bryce, M. R.; Petty, M. C.; Moloney, J.; Howard, J. A. K.; Joyce, M. J.; Port, S. N. *J. Org. Chem.* **2000**, *65*, 8269.
(31) Liu, H.; Liu, S.-G.; Echegoyen, L. *Chem. Commun.* **1999**, 1493.
(32) Liu, S.-G.; Liu, H.; Bandyopadhyay, K.; Gao, Z.; Echegoyen, L. *J. Org. Chem.* **2000**, *65*, 3292.
(33) Cooke, G.; Duclairoir, F. M. A.; Rotello, V. M.; Stoddart, J. F. *Tetrahedron Lett.* **2000**, *41*, 8163.
(34) Bryce, M. R.; Cooke, G.; Duclairoir, F. M. A.; John, P.; Perepichka, D. F.; Polwart, N.; Rotello, V. M.; Stoddart, J. F.; Tseng, H.-R. *J. Mater. Chem.* **2003**, *13*, 2111.
(35) Kuo, K.-N.; Moses, P. R.; Lenhard, J. R.; Green, D. C.; Murray, R. W. *Anal. Chem.* **1979**, *51*, 745.
(36) Sandroff, C. J.; Weitz, D. A.; Chung, J. C.; Herschbach, D. R. *J. Phys. Chem.* **1983**, *87*, 2127.
(37) Everett, W. R.; Fritsch-Faules, I. *Anal. Chim. Acta* **1995**, *307*, 253.
(38) Volante, R. P. *Tetrahedron Lett.* **1981**, *22*, 3119.
(39) Simonsen, K. B.; Svenstrup, N.; Lau, J.; Simonsen, O.; Mørk, P.; Kristensen, G. J.; Becher, J. *Synthesis* **1996**, 407.
(40) Knoll, W. *Annu. Rev. Phys. Chem.* **1998**, *49*, 569.
(41) Kretschmann, E.; Raether, H. *Z. Naturforsch. A* **1968**, *23*, 2135.
(42) Aust, E. F.; Ito, S.; Sawodny, M.; Knoll, W. *Trends Polym. Sci.* **1994**, *2*, 313.
(43) Raether, H. *Surface Plasmons on Smooth and Rough Surfaces and on Gratings*; Springer Tracts in Modern Physics; Springer-Verlag: Berlin, 1988; Vol. 111.
(44) Tamada, K.; Ishida, T.; Knoll, W.; Fukushima, H.; Colorado, R., Jr.; Graupe, M.; Shmakova, O. E.; Lee, T. R. *Langmuir* **2001**, *17*, 1913.
(45) Yokokawa, S.; Tamada, K.; Ito, E.; Hara, M. *J. Phys. Chem. B* **2003**, *107*, 3544.
(46) Trasatti, S.; Petrii, O. A. *Pure Appl. Chem.* **1991**, *63*, 711.
(47) Suenaga, M. *J. Comput. Chem. Jpn.* **2005**, *4*, 25.
(48) Peterlinz, K. A.; Georgiadis, R. *Langmuir* **1996**, *12*, 4731.
(49) Yokota, Y.; Yuge, R.; Miyazaki, A.; Enoki, T.; Hara, M. *Mol. Cryst. Liq. Cryst.* **2003**, *407*, 517.
(50) Porter, M. D.; Bright, T. B.; Allara, D. L.; Chidsey, C. E. D. *J. Am. Chem. Soc.* **1987**, *109*, 3559.
(51) Bain, C. D.; Troughton, E. B.; Tao, Y.-T.; Evall, J.; Whitesides, G. M.; Nuzzo, R. G. *J. Am. Chem. Soc.* **1989**, *111*, 321.
(52) Miura, Y. F.; Tovar, G. E. M.; Ohnishi, S.; Hara, M.; Sasabe, H.; Knoll, W. *Thin Solid Films* **2001**, *393*, 225.
(53) Atkins, P. W. *Physical Chemistry*, 6th ed.; Oxford University Press: Oxford, U.K., 1998.
(54) Seed, A. J.; Toyne, K. J.; Goodby, J. W. *Liq. Cryst.* **2001**, *28*, 1047.
(55) Tamada, K.; Akiyama, H.; Wei, T. X. *Langmuir* **2002**, *18*, 5239.
(56) Bard, A. J.; Faulkner, L. R. *Electrochemical Methods: Fundamentals and Applications*, 2nd ed.; John Wiley & Sons: New York, 2001.
(57) Brown, A. P.; Anson, F. C. *Anal. Chem.* **1977**, *49*, 1589.
(58) Sato, Y.; Uosaki, K. In *Proceedings of the Fifth International Symposium on Redox Mechanisms and Interfacial Properties of Molecules of Biological Importance*; Schultz, F. A., Taniguchi, I., Eds.; The Electrochemical Society: Pennington, NJ, 1993; pp 299−310.